Transport properties of the two-dimensional electron gas in AlP quantum wells at zero temperature

A. Gold* and R. Marty
Centre d'Elaboration de Materiaux et d'Etudes Structurales (CEMES-CNRS), 29 Rue Jeanne Marvig, 31055 Toulouse, France
(Received 22 June 2007; revised manuscript received 23 August 2007; published 11 October 2007)

Due to strain and confinement effects, the two-dimensional electron gas in AlP has a valley degeneracy $g_v=1$ for quantum well width $L<L_c=45.7$ Å and a valley degeneracy of $g_v=2$ for quantum well width $L>L_c$. We present theoretical results for transport properties of the electron gas for the two cases. We calculate the mobility of the two-dimensional electron gas at zero temperature for interface-roughness scattering and for impurity scattering. We discuss the transport scattering time, the single-particle relaxation time, and the magnetoresistance in a parallel magnetic field. Our calculations are important (i) for the design of AlP quantum well structures, (ii) to get insight into relevant microscopic parameters of different scattering mechanisms, and (iii) to obtain information about the electronic properties of the electron gas at low density where many-body effects and localization effects are important.

DOI: 10.1103/PhysRevB.76.165309 PACS number(s): 73.43.Qt, 73.63.Hs, 73.50.−h, 73.61.Ey

I. INTRODUCTION

GaP/AlP/GaP quantum well (QW) structures and multiple quantum well structures, where the electron gas is located in the AlP, have been grown and studied recently at low temperature via cyclotron resonance, quantum Hall effect, Shubnikov–de Haas oscillations[1] (SdH) and intersubband spectroscopy.[2] The system is similar to the $Al_xGa_{1-x}As/AlAs/Al_xGa_{1-x}As$ system, which was studied for the past years; for a review, see Ref. 3. In this paper, we present theoretical results for transport properties of the two-dimensional electron gas, which is present in the structure GaP/AlP/GaP. We discuss two scattering mechanisms, interface-roughness scattering (IRS) and charged impurities scattering (CIS), and three different scattering times, for the conductivity and for transport in a weak perpendicular magnetic field and in a strong parallel magnetic field.

Consider the surface of AlP in the (001) direction. The energy minimum is at the X point of the Brillouin zone; therefore, there exists a threefold level degeneracy.[1,4] Due to biaxial strain (st) present in the AlP layer, there exists a splitting of the energy minimum to a twofold level and a onefold level. The twofold level is lower in energy than the onefold level. This strain induced energy splitting, $\Delta E_{st}=40$ meV, gives rise to two bands, one with $g_v=2$ (g_v is the valley degeneracy) and one with $g_v=1$.[1] The two bands are characterized by different effective masses, which are the mass in the z direction m_c (the confinement mass) and the mass m^* in the xy direction (transport mass). In the following, we suppose that one has introduced electrons in the AlP layer by doping with donors or via a gate. In an AlP layer of finite width, one has to add the confinement effects for the electron gas. We suppose a QW of width L and infinite confinement. The confinement effects give rise to energy levels $E_n^{QW}=\hbar^2\pi^2n^2/2m_cL^2$, with $n\in N^+$ and different masses in the z direction. These QW energies are the origin of the subband structure associated with each of the two bands. It shall be argued later in detail that the electron gas in the lowest subband has valley degeneracy $g_v=1$ for wells of width $L<L_c$ and valley degeneracy $g_v=2$ for wells of width $L>L_c$.[1]

In this paper, we present for zero temperature some calculations for the mobility in such structures. We consider a simple model of quantum wells with infinite confinement.[6,7] This model was formulated some time ago in order to discuss transport properties of the two-dimensional electron gas in $Si/Si_{1-x}Ge_x$ QWs. We think that our calculations will help sample growers to design samples with interesting physical properties. We present results for the mobility, results concerning the Dingle temperature (the single-particle relaxation time) and the magnetoresistance in a parallel magnetic field. Such measurements can be used to get information on the real doping profile of the sample and microscopic parameters of the disorder. In the last part of the paper, we discuss the possibility of a metal-insulator transition (MIT) which might happen in QW at low density.

The paper is organized as follows. In Sec. II, we describe the model for the QW and the theory which we shall use for our calculations. In Sec. III, we present results for IRS. Our results for CIS are presented in Sec. IV. In Sec. V, we describe the MIT in quantum wells. We discuss our results in Sec. VI and conclude in Sec. VII.

II. MODEL AND THEORY

A. Model and electronic structure

We consider a two-dimensional electron gas with parabolic dispersion determined by the effective mass m^*. We assume that the electron gas is in the xy plane with infinite confinement for $z<0$ and $z>L$. For $0\leqslant z\leqslant L$, the electron gas in the lowest subband is described by the wave function $\Psi(0\leqslant z\leqslant L)=\sqrt{2/L}\sin(\pi z/L)$. In this QW model, form factors for IRS, CIS, and the electron-electron interaction were calculated in analytical form before[7] and are not given explicitly in this paper. For the background dielectric constant of AlP, we use $\varepsilon_L=9.8$. The QW is shown in a schematic view in the inset of Fig. 1.

The longitudinal mass $m_l=0.9m_e$ and the transverse mass $m_t=0.3m_e$ in AlP have been determined in experiment.[1,2,5] m_e is the free electron mass. This means that for (001) grown

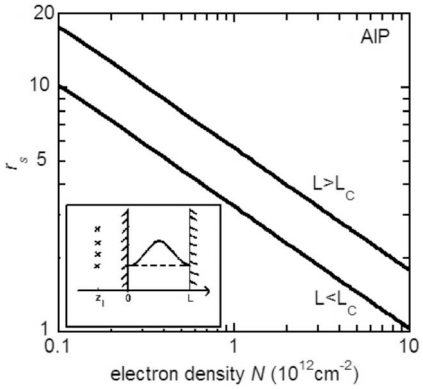

FIG. 1. Wigner-Seitz parameter r_s versus electron density N for $L<L_c$ (with Bohr radius $a^*=17.3$ Å) and $L>L_c$ ($a^*=10.0$ Å). In the inset, we show a schematic representation of a quantum well of width L and position z_i of the impurity layer.

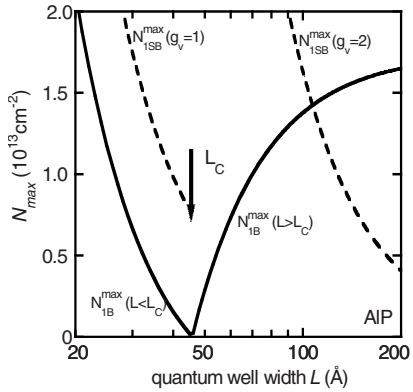

FIG. 2. Density $N_{\max}$ for the application of a one-band (1B) and a one-subband (1SB) model versus quantum well width L. Shown are $N_{1B}^{\max}(L<L_c)$, $N_{1B}^{\max}(L>L_c)$, $N_{1SB}^{\max}(g_v=1)$, and $N_{1SB}^{\max}(g_v=2)$.

material and QWs of width $L<L_c$, the transport mass m^* is $m^*=0.3m_e$, while the mass in the z direction is $m_c=0.9m_e$.[5] Note that the transport mass connects the mobility μ with the transport scattering time τ_t: $\mu=e\tau_t/m^*$. For QWs of width $L>L_c$, one gets $m^*=0.52m_e=(m_l m_t)^{1/2}$ and $m_c=0.3m_e$.[1] With these parameters, the critical length is determined by $L_c=\sqrt{[(m_l-m_t)/2m_l m_t](\pi^2\hbar^2/\Delta E_{st})}=45.7$ Å. Presently grown QWs have widths in the range 20 Å$\leqslant L\leqslant$150 Å with electron density $N<1\times10^{13}$ cm^{-2}, which implies that QWs with $L<L_c$ and $L>L_c$ can be studied experimentally.

In the following, we study the cases $L<L_c$ and $L>L_c$. For $L<L_c$, we use $g_v=1$, $m_c=0.9m_e$, and $m^*=0.3m_e$.[5] The effective Bohr radius a^* is defined with the transport mass and the background dielectric constant and is given by $a^*=17.3$ Å. For $L>L_c$, we use $g_v=2$, $m_c=0.3m_e$, and $m^*=0.52m_e$.[1] The effective Bohr radius in this case is smaller because of the larger mass and is given by $a^*=10.0$ Å.

We introduce the Wigner-Seitz parameter r_s via $r_s=1/\sqrt{\pi N a^{*2}}$, and this parameter gives information about the importance of many-body effects. r_s versus electron density is shown in Fig. 1 for QWs with $L<L_c$ and $L>L_c$. For a given electron density, r_s is larger for $L>L_c$ due to the smaller effective Bohr radius. In the simple picture of one occupied subband and taking into account interaction effects, one expects that many-body effects become important for $r_s>1$, see Fig. 1 for the corresponding electron density.

We study an electron gas in a quantum well with infinite confinement where only one band and only one subband are occupied. For $L<L_c$, the (second) band with $g_v=2$ is higher in energy than the (first) band with $g_v=1$. If the Fermi energy ε_F of the band with $g_v=1$ exceeds the difference in energy between the two bands, we begin to populate the second band. This criterion gives a maximal density $N_{1B}^{\max}(L<L_c)$ in order to have only one band (1B) occupied. For $L>L_c$, the (first) band with $g_v=1$ is higher in energy than the (second) band with $g_v=2$ and the electron density should be smaller than the maximal density $N_{1B}^{\max}(L>L_c)$ in order to have only one band occupied. A simple calculation for infinite quantum wells gives

$$N_{1B}^{\max}(L<L_c)=1.05\times10^{16}\ \text{cm}^{-2}\ \text{Å}^2/L^2-5.02\times10^{12}\ \text{cm}^{-2} \tag{1a}$$

for $L<L_c$ and

$$N_{1B}^{\max}(L>L_c)=1.74\times10^{13}\ \text{cm}^{-2}-3.63\times10^{16}\ \text{cm}^{-2}\ \text{Å}^2/L^2 \tag{1b}$$

for $L>L_c$. Note that $N_{1B}^{\max}(L\to\infty)=1.74\times10^{13}$ cm^{-2}, which corresponds to $\Delta E_{st}=40$ meV$=\varepsilon_F$.

In order to have only one subband (1SB) occupied, the Fermi energy must be smaller than the intersubband energy (ise) distance of the QW, given by $\Delta E_{QW}^{ise}=3\hbar^2\pi^2/2m_c L^2$. For the band with $g_v=1$ for $L<L_c$, this corresponds to a maximal electron density

$$N_{1SB}^{\max}(g_v=1)=1.57\times10^{16}\ \text{cm}^{-2}\ \text{Å}^2/L^2. \tag{2a}$$

For the band with $g_v=2$ for $L>L_c$, we find

$$N_{1SB}^{\max}(g_v=2)=1.63\times10^{17}\ \text{cm}^{-2}\ \text{Å}^2/L^2. \tag{2b}$$

The density range where only 1B and only 1SB are occupied is the region

$$0<N<\min[N_{1B}^{\max},N_{1SB}^{\max}]. \tag{3}$$

In Fig. 2, we show $N_{1B}^{\max}$ and $N_{1SB}^{\max}$ versus quantum well width. Note that the range for one occupied band and one occupied subband is quite large ($N^{\max}\approx1\times10^{13}$ cm^{-2}) if one is not near L_c. For $L=L_c$, one has $N^{\max}=0$, and one has to consider a system where the two bands with $g_v=1$ and $g_v=2$ are populated simultaneously and have the same Fermi energy.

B. Disorder, screening, and transport theory

We consider in this paper interface-roughness and randomly distributed charged impurities as source of disorder. Detailed results for the random potential due to different kinds of disorder can be found in Ref. 7. We present results for the mobility for zero temperature, determined by the transport scattering time τ_t, and the single-particle relaxation time τ_s, which can be measured by SdH oscillations in a

weak perpendicular magnetic field.[4] For a discussion of the single-particle relaxation time τ_s, see Refs. 8 and 9. For the transport scattering time, backscattering is most important while small angle scattering is less important. For the single-particle relaxation time, all scattering events contribute with the same weight.

The interaction effects of the electron gas and the screening are treated within the random-phase approximation (RPA) with a finite local-field correction (LFC).[4,7,9] The LFC $G(q)$ describes many-body effects (exchange and correlation) beyond the mean-field approximation (the RPA) and becomes important for low electron density.[10] We use the Hubbard approximation $G_H(q)=q/(g_s g_v\sqrt{k_F^2+q^2})$ in our calculation for the screening function. g_s is the spin degeneracy. In the Hubbard approximation, correlation effects are neglected. However, in using $G_H(q)$, we show that it is important to take into account the physics described by the LFC. For the unpolarized electron gas, we apply $g_s=2$, and for the fully polarized electron gas, we use $g_s=1$.

By applying a parallel magnetic field, the electron gas can be spin polarized. The density of states and the screening properties are modified in a parallel magnetic field, and this gives rise to a magnetoresistance.[11] The parallel magnetic field induces a Zeeman splitting of spin-up and spin-down electrons, and for $B \geqslant B_c=2hN/(eg_v g^* m^*/m_e)$, the system is completely spin polarized. g^* is the Lande g factor and h the Planck constant. Orbital effects are neglected in our calculation; therefore, we have, in our approach, $\rho(B>B_c)=\rho(B_c)$.[11] In this paper, we only discuss the resistance ratio $\rho(B=B_c)/\rho(B=0)$. A partially polarized two-dimensional electron gas in AlP for $0<B<B_c$ shall be discussed elsewhere.

In some figures, we present ratios, for instance, τ_t/τ_s and $\rho(B=B_c)/\rho(B=0)$. In such ratios, the parameter Δ cancels out for IRS, and for CIS, the impurity N_i concentration cancels out. However, this is only the case if one scattering mechanism is present. In experiment, sometimes two scattering mechanisms are important and then one should be more careful in analyzing the data.

III. RESULTS FOR INTERFACE-ROUGHNESS SCATTERING

It was predicted from theory, see Fig. 3 of Ref. 6, that IRS is the dominant scattering mechanism in thin quantum wells and that the mobility increases as $\mu \propto L^6$. This law was confirmed later in experiments on narrow GaAs (Refs. 12 and 13) and InAs (Ref. 14) quantum wells. For more references on experimental results concerning IRS in quantum wells, see Ref. 14. We neglect in this paper the penetration effects of the wave function into the barrier.

The Fourier transform of the random potential for IRS is proportional to $m^{*2}\Delta^2\Lambda^2/(m_c^2 L^6)$ and consequently one obtains $\mu \propto L^6$. Δ represents the average height of the roughness in the z direction and Λ the correlation length parameter of the roughness in the xy direction.[4] Note that the mobility is given by the relation $\mu \propto m_c^2 L^6 \exp(-k_F^2\Lambda^2)/(m^{*2}\Delta^2\Lambda^2)$. k_F is the Fermi wave number. IRS in quantum wells with width $L<L_c$ is reduced due to mass effects by a factor $(m^*/m_c)^2 \approx (0.3/0.9)^2=1/9$, while for $L>L_c$, it is enhanced due to mass effects by a factor $(m^*/m_c)^2 \approx (0.52/0.3)^2 \approx 3$.[6] Therefore, we believe that IRS may also be important in quantum wells with $L_c<L<2L_c$. In thin QW, however, IRS is certainly very important. Some more results on IRS for $L<L_c$ will be published elsewhere.[15]

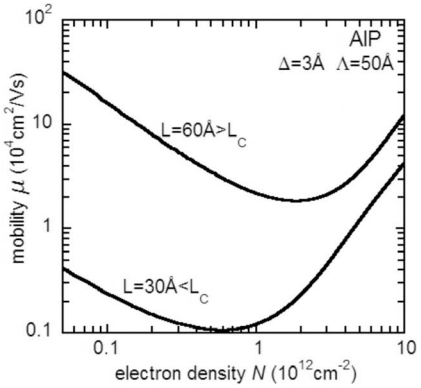

FIG. 3. Mobility μ versus electron density N for a quantum well of width $L=30$ Å $<L_c$ and $L=60$ Å $>L_c$ for IRS with $\Delta=3$ Å and $\Lambda=50$ Å. The LFC in the Hubbard approximation has been taken into account.

A representative example for the case of IRS is shown in Fig. 3. As parameters of the interface roughness, we used $\Delta=3$ Å and $\Lambda=50$ Å. For $N<N^*$ and with increasing electron density, the mobility first decreases, reaches a minimum near $N^* \approx g_v/(2\pi\Lambda^2)=g_v(6.37\times 10^{11}\ \mathrm{cm}^{-2})$, and increases again for $N>N^*$.[7] For $\Lambda=50$ Å, the results shown in Fig. 3 can be used by experimentalists to obtain the mobility for different QW widths by applying $\mu(L,N) \equiv \mu_1(L_1,N)(L_1/L)^6$ with $L_1=30$ Å for $L<L_c$ and $\mu(L,N) \equiv \mu_2(L_2,N)(L_2/L)^6$ with $L_2=60$ Å for $L>L_c$.

The single-particle relaxation time τ_s can be measured because τ_s is related to the Dingle temperature T_D via $k_B T_D=\hbar/2\pi\tau_s$. The ratio of the transport scattering time and the single-particle relaxation time, τ_t/τ_s, versus electron density is shown in Fig. 4 for $L=60$ Å. Results including the LFC are shown as the solid line and without the LFC as the dashed-dotted line. Only small effects due to the LFC are seen. We mention that the results for the ratio τ_t/τ_s for different well widths are nearly independent of the QW width. The reason is that all the effects of form factors are nearly canceled in the ratio. Note the larger ratio at higher electron density due to reduced backscattering in the transport scattering time τ_t: $\tau_t/\tau_s=(k_F\Lambda)^2/3$.[9] The ratio allows us to determine $k_F\Lambda$, and for a given density, the parameter Λ can be determined. The ratio $\tau_t/\tau_s=2/3$ for small electron density $(k_F\Lambda \ll 1)$ is characteristic for IRS.[9]

We now discuss the prediction for the resistance in a parallel magnetic field. The resistance ratio $\rho(B_c)/\rho(B=0)$ versus electron density for $L=60$ Å $>L_c$ for IRS is shown in Fig. 5. The ratio $\rho(B_c)/\rho(B=0)$ is large when the density is low. The LFC is important in the low density limit and can substantially increase the ratio $\rho(B_c)/\rho(B=0)$ compared to the case where the LFC is neglected. Without LFC, the limiting behavior for small density is $\rho(B_c)/\rho(B=0)=8$.[11] If one trusts in the concept and the physics represented by the LFC,

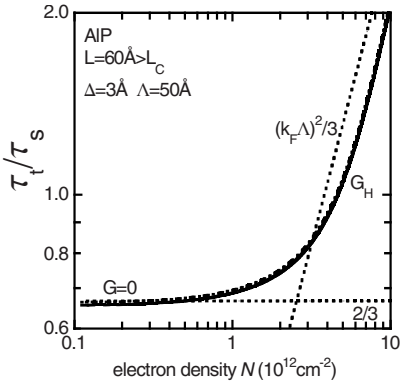

FIG. 4. Ratio τ_t/τ_s versus electron density N for a quantum well of width $L=60$ Å $>L_c$ for IRS with $\Delta=3$ Å and $\Lambda=50$ Å. The solid line represents the calculation with the LFC in the Hubbard approximation taken into account, and the dashed-dotted line is without the LFC. The dotted lines represent analytical results from Ref. 9.

one can use measurements of the magnetoresistance to obtain information about the LFC.

IV. RESULTS FOR CHARGED IMPURITY SCATTERING

Let us first note that CIS is characterized by the impurity density N_i and the distance z_i of the impurity layer from the QW edge at $z=0$, see the inset of Fig. 1. For $z_i=0$, the impurities are at the interface of the QW, and for $z_i=L/2$, the impurities are at the center of the QW (residual impurities). For $z_i<0$, the impurities are outside the QW (remote doping). In order to assure neutrality, we have assumed that $N_i=N$. However, we want to stress that $\mu\propto 1/N_i$, and the figures can be used to derive the mobility as function of electron density for fixed N_i. For instance, for given $\mu^{\exp}$ and given electron density N and QW width, one can calculate $N_i^{\exp}=N_i\mu/\mu^{\exp}$, with $N_i=N$ and μ from our figures, assuming that a single scattering mechanism is present. This is important for cases where the electron density is varied by a gate.

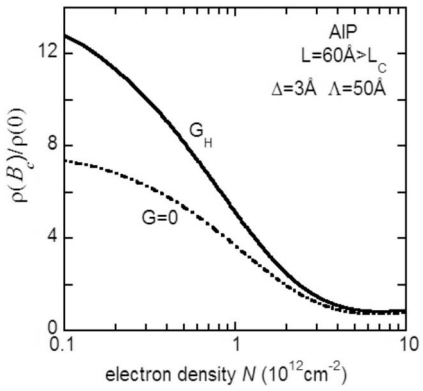

FIG. 5. Resistance ratio $\rho(B_c)/\rho(B=0)$ versus electron density N for a quantum well of width $L=60$ Å $>L_c$ for IRS with $\Delta=3$ Å and $\Lambda=50$ Å. The solid line represents the calculation where the LFC in the Hubbard approximation is taken into account and the dashed-dotted line is without LFC.

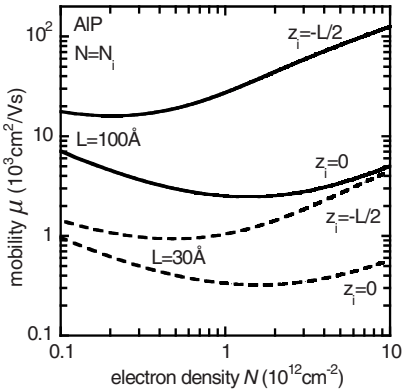

FIG. 6. Mobility μ versus electron density N for a quantum well of width $L=30$ Å $<L_c$ and $L=100$ Å $>L_c$ for CIS with $N_i=N$ for two different positions $z_i=0$ and $z_i=-L/2$ of the impurities. The LFC in the Hubbard approximation has been taken into account.

The random potential which we use in this section is for charged impurities distributed randomly in the xy plane. The form factor for CIS was given in Ref. 7 in analytical form as function of q, L, and z_i. The expression for the mobility can be found in Ref. 9. The results given in this section are in lowest order of the impurity concentration.

A. Mobility and conductivity measurements

A representative example is shown in Fig. 6 where the mobility versus density for two different QW widths, $L=100$ Å and $L=30$ Å, is shown for impurities outside the well ($z_i=-L/2$) and at the interface of the QW ($z_i=0$). The density dependence of the mobility for $N_i=N$ is not dramatic; however, the width plays an important role. For larger width, the distance of the impurity layer to the $\sin^2(\pi z/L)$ profile of the electron gas in the z direction is larger; therefore, the mobility increases. For impurities outside the QW, the mobility is much higher than for impurities in the QW; this is the well-known remote doping effect.

Our results for the mobility versus QW width are shown in Fig. 7 for $N=N_i=1\times10^{12}$ cm^{-2} and in Fig. 8 for $N=N_i$

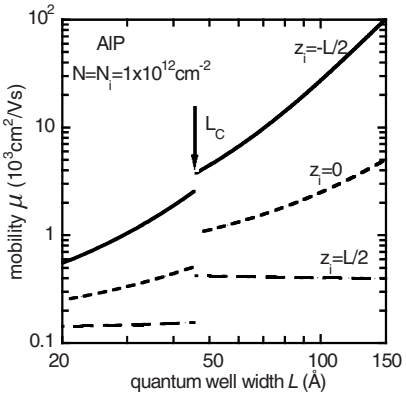

FIG. 7. Mobility μ versus quantum well width L for CIS for $N=N_i=1\times10^{12}$ cm^{-2} and three different values of the position of impurities z_i. The LFC in the Hubbard approximation has been taken into account.

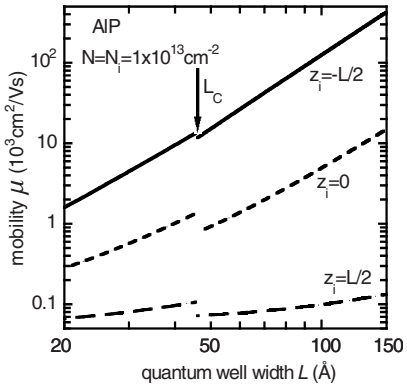

FIG. 8. Mobility μ versus quantum well width L for CIS for $N=N_i=1\times10^{13}$ cm^{-2} and three different values of the position of impurities z_i. The LFC in the Hubbard approximation has been taken into account.

$=1\times10^{13}$ cm^{-2}. For $z_i\leqslant0$, the mobility increases with increasing well width. The reason for this was already discussed—the distance between the electron gas and the impurity layer increases with increasing well width. For $z_i=L/2$, we see a very weak QW width dependence of the mobility. Most impressive is the weak change at $L=L_c$ for larger electron density, see Fig. 8. This comes from the fact that the larger screening in the QW for $L>L_c$ compensates the larger effective mass compared to the QW with $L<L_c$. For samples where one can change the electron density with a gate, the impurity density is fixed and the mobility values are higher than shown in Fig. 8 where we have used $N=N_i=1\times10^{13}$ cm^{-2}.

B. Single-particle relaxation time: Shubnikov–de Haas oscillations

We repeat that N_i is canceled out in the ratio τ_t/τ_s. However, in order to obtain the ratio, one needs the two numbers for τ_t and τ_s; thus, two measurements are necessary. The absolute value of τ_t allows us to get an idea about the scattering mechanisms present in the sample.

The ratio τ_t/τ_s versus electron density is shown in Fig. 9 for impurities at the center of the QW at $z_i=L/2$ (residual impurities). With increasing electron density, the ratio increases smoothly. For impurities located in the center of the QW, the enhancement with increasing density is not very strong; see the linear scale for τ_t/τ_s in Fig. 9. With increasing electron density, the ratio increases smoothly from 1 to about 2 for $N=1\times10^{13}$ cm^{-2}. A finite LFC decreases the ratio.

Results for τ_t/τ_s versus electron density are shown in Fig. 10 for impurities outside the QW (remote doping) at $z_i=-L/2$. In fact, for an ideal electron gas with $L=0$, one finds the analytical result $\tau_t/\tau_s=4k_F^2|z_i|^2$.[9] In the more general case of a QW with finite width, one should add to z_i the distance $L/2$ for the QW. Therefore, for high density, on finds the analytical result $\tau_t/\tau_s=4k_F^2(L/2+|z_i|)^2$, which becomes $\tau_t/\tau_s=4k_F^2L^2$ if $z_i=-L/2$. This result is also shown in Fig. 10 as the dotted line. We suggest that measurements of τ_t and τ_s at higher density allow to determine z_i.

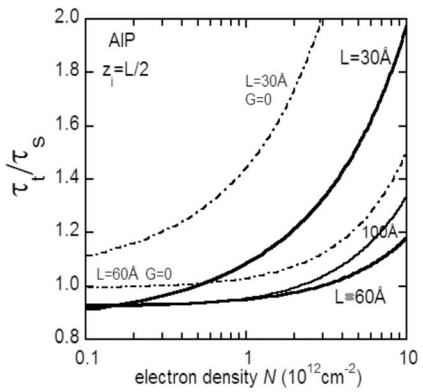

FIG. 9. Ratio τ_t/τ_s versus electron density N for CIS for impurities at the center of the QW $z_i=L/2$ and for quantum wells of different widths. The solid lines represent the calculation with the LFC in the Hubbard approximation and the dashed-dotted lines without LFC.

C. Transport properties of the spin-polarized electron gas for $B\geqslant B_c$

The ratio $\rho(B=B_c)/\rho(B=0)$ versus electron density is shown in Fig. 11 for impurities at the center of the QW ($z_i=L/2$). With decreasing density, the ratio increases strongly. Without LFC, the ratio varies between $0.5<\rho(B=B_c)/\rho(B=0)<4$, the dashed lines.[11] Including the LFC strongly increases the ratio, especially for $L<L_c$. Again, we see a very strong effect of a finite LFC at low density. For $L>L_c$, the ratio is only weakly L dependent; compare in Fig. 11 the results for $L=60$ Å and $L=100$ Å.

In Fig. 12, we show $\rho(B=B_c)/\rho(B=0)$ versus quantum well width L for different electron densities for $z_i=L/2$ (residual impurities). The differences at $L=L_c$ are considerable. Note the large enhancement of $\rho(B=B_c)/\rho(B=0)$ for low density. We note a weak quantum well width dependence for $L<L_c$ and $L>L_c$.

In Fig. 13, we show $\rho(B=B_c)/\rho(B=0)$ versus well width for different electron densities for impurities outside the well

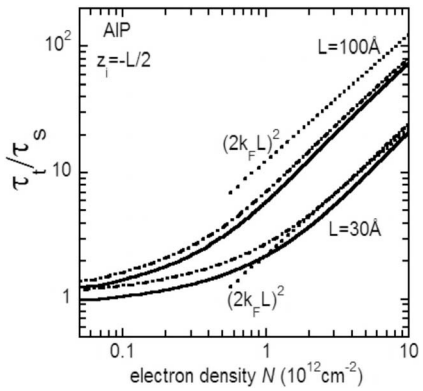

FIG. 10. Ratio τ_t/τ_s versus electron density N for CIS for impurities outside the QW with $z_i=-L/2$ and for quantum wells of different widths. The solid lines represent the calculation with the LFC in the Hubbard approximation and the dashed-dotted lines without LFC. The dotted lines represent the analytical result $(2k_FL)^2$ of Ref. 9; see the discussion in text.

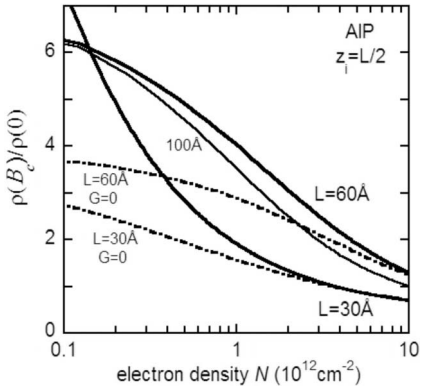

FIG. 11. Resistance ratio $\rho(B_c)/\rho(B=0)$ versus electron density N for CIS for $z_i=L/2$ and quantum wells of different widths $L=100$ Å $>L_c$, $L=60$ Å $>L_c$, and $L=30$ Å $<L_c$. The solid lines represent the calculation where the LFC in the Hubbard approximation is taken into account and the dashed-dotted lines represent the calculation without LFC.

$z_i=-L/2$ (remote doping). While one does not see a dramatic difference between Fig. 12, where impurities are at the center of the QW, and Fig. 13, where impurities are outside the well, the quantum well width dependence is stronger in Fig. 13 for impurities outside the well than for impurities inside the well. In addition, $\rho(B=0)$ is quite different in the two cases.

V. RESULTS FOR THE METAL-INSULATOR TRANSITION

Using a mode-coupling theory, a MIT was predicted[6] in quantum wells. This MIT corresponds to a phase transition where interaction effects become, for low electron density, inefficient to screen the random potential created by the disorder. Weak-localization effects are neglected in this theory. In the mode-coupling theory, multiple-scattering events together with screening effects are taken into account, and this leads to a MIT with a metallic phase at high electron density and an insulating phase at low electron density.[16] The critical electron density N_c for the MIT in our theory is the density

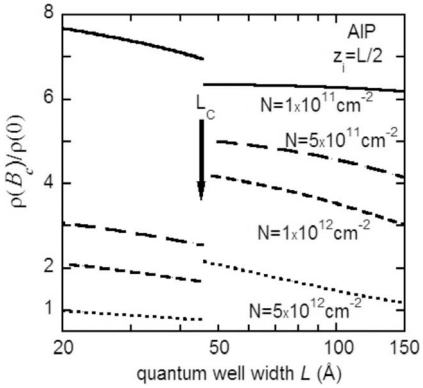

FIG. 12. Resistance ratio $\rho(B_c)/\rho(B=0)$ versus quantum well width L for CIS for $z_i=L/2$ (impurities in the well) and different densities. The LFC in the Hubbard approximation is taken into account.

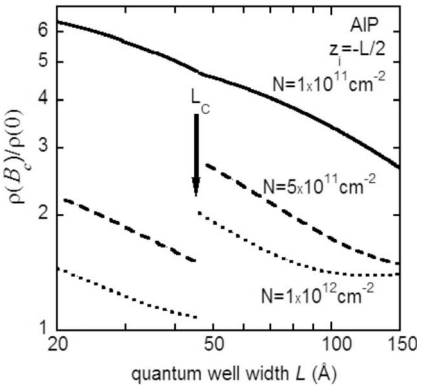

FIG. 13. Resistance ratio $\rho(B_c)/\rho(B=0)$ versus quantum well width L for CIS for $z_i=-L/2$ (remote doping) and different densities. The LFC in the Hubbard approximation is taken into account.

where strong localization effects are expected.

For IRS and CIS, an insulating phase is expected for $N<N_c$ and a conducting phase for $N>N_c$. The critical electron density of the quantum well for IRS depends on the width of the QW and decreases with increasing quantum well width, because IRS is less important for larger QW width. Numerical results for N_c versus QW width L for AlP are shown in Fig. 14. For the solid lines, only IRS was taken into account. We conclude that for QWs with $L>1.5L_c$, the IRS is not anymore important. Due to the mass ratio, the IRS for given QW width is more important for $L>L_c$ than for $L<L_c$. This is clearly seen in Fig. 14; compare the two solid lines, both calculated for IRS.

Results for N_c for impurities outside the QW with $z_i=-L/2$ and $N_i=N$ (remote doping), together with IRS, are also shown in Fig. 14. For $L>L_c$, remote doping increases N_c appreciably, compared to IRS alone. For impurities at $z_i=L/2$ and $N_i=1\times10^{11}$ cm^{-2} (residual impurities) and IRS, the phase diagram is also shown in Fig. 14. For $L>L_c$, one finds that $N_c\cong2\times10^{11}$ cm^{-2} is nearly independent of the

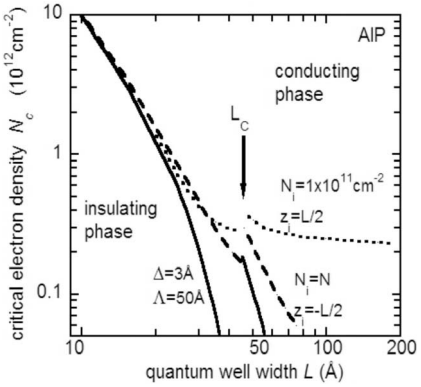

FIG. 14. Critical electron density N_c for a conducting phase ($N>N_c$) and an insulating phase ($N<N_c$) versus quantum well width L. For the solid lines, only IRS with $\Delta=3$ Å and $\Lambda=50$ Å is taken into account. For the dashed lines, CIS with $z_i=-L/2$ and $N_i=N$ (remote doping) and IRS with $\Delta=3$ Å and $\Lambda=50$ Å are used. For the dotted lines, CIS with $z_i=L/2$ and $N_i=1\times10^{11}$ cm^{-2} (residual impurities) and IRS with $\Delta=3$ Å and $\Lambda=50$ Å are taken into account.

QW width. Of course, if one reduces N_i, one also reduces N_c. We conclude that for $L > L_c$, residual impurities in the QW determine the critical density N_c, which is relatively independent of the QW width. As a rough estimate for residual impurities and $L > L_c$, we obtain from our numerical results $N_c \approx 2N_i$, see the dotted line in Fig. 14 for $L > L_c$.

From Fig. 14, we predict that quantum wells of width L grown with $N \leqslant N_c$ will be insulating. Increasing the electron density, for instance, by light, doping, or a gate, could bring the two-dimensional electron gas back into the metallic regime. However, for $L < L_c$, the increase in electron density must be substantial. For $L > L_c$, the electron density should fulfill the relation $N > 2N_i$ for being in the metallic regime. We suggest more experiments with QWs with small width in order to better understand the insulating phase apparently present at high density due to the strong IRS. The prediction of this phase transition should be taken seriously; the prediction of the L^6 law for the mobility was also verified in experiment. From our theoretical results, we conclude that with IRS, one should very rapidly approach the regime of strong disorder by reducing the QW width.

Near the MIT, multiple-scattering effects have to be taken into account for the mobility. A generalized expression for the mobility is described[17] by $\mu_{MIT}(N > N_c) = \mu(1 - N_c/N)$ and $\mu_{MIT}(N < N_c) = 0$. μ represents the mobility calculated in lowest order of the random potential, as shown in Figs. 3 and 6–8, and N_c is the critical density shown in Fig. 14. Note that $\mu_{MIT}(N \gg N_c) \approx \mu$.

VI. DISCUSSION

Measurements of the magnetoresistance and of SdH oscillations are complementary. The determination of τ_t/τ_s is most interesting for large electron density where the concept of a Fermi liquid is well defined and where SdH oscillations exist for weak disorder. Nevertheless, one can get information about the disorder parameters Δ and z_i. The ratio $\rho(B = B_c)/\rho(B = 0)$ is more interesting for low electron density, where many-body effects are important and where one needs to test the concept of a Fermi liquid. In principle, it is possible to obtain information about the many-body effects via the LFC.

Measurements of SdH oscillations have recently been used to show that the effective mass in silicon (100) is diverging at low electron density.[18] The origin of this divergence is not yet known. Together with the effective mass, the Dingle temperature is determined in SdH measurements. This example shows that measurements of SdH oscillations allow us to discover unexpected physical phenomena. Moreover, the determination of τ_t/τ_s can be used to determine microscopic parameters of disorder. This is important for sample growers in order to compare the real doping profile with the intended doping profile in the case of charged impurities. In the case of IRS, the microscopic parameter Λ can be determined for thin QWs with $L < L_c$. A determination of Λ with τ_t/τ_s was recently performed[19] for the two-dimensional electron gas in $Al_xGa_{1-x}N/GaN$ heterostructures and a value $\Lambda = 100$ Å was estimated from experimental results.

The determination of Δ and Λ for QWs with $L < L_c$, where IRS is dominant, would allow us to estimate if interface roughness scattering is also important for QWs with $L > L_c$, supposing that the roughness parameters are independent of the QW width. The single-particle relaxation time, together with the transport scattering time, is the essential quantity in order to study the microscopic parameters of disorder in the case of a Fermi liquid at high density, where the Wigner-Seitz parameter is not too large and where $k_F\Lambda > 1$ and $k_F(L/2 + |z_i|) > 1$.

The application of a parallel magnetic field allows us to spin polarize the electron gas. This gives rise to density of states modifications and reduced screening.[11] A Fermi-liquid concept was applied to calculate the magnetoresistance for weak disorder. Also, for strong disorder, near the MIT, some predictions have been made, and the importance of strong many-body effects in the low density limit has been discussed within the concept of a local-field correction.[17] Therefore, we argue that agreement with predictions made in Refs. 11 and 17 would imply the confirmation of the Fermi-liquid concept together with the existence of a MIT. In addition, we argue that the local-field correction in the strongly correlated regime can be estimated with $\rho(B = B_c)/\rho(B = 0)$ measurements. The low density behavior can be studied with low magnetic fields. We believe that such measurements can be made in many laboratories if clean samples are available, where the metal-insulator occurs at low electron density. Otherwise, one could study the behavior of the MIT with a parallel magnetic field. We mention that after about 25 years of discussion, the existence of a MIT in two-dimensional electron systems is quite well established now.[20,21]

Finally, we give the expressions of the critical magnetic field for complete spin polarization. For $L > L_c$, the Lande g factor g^* was determined in experiment and found to be $g^*(L > L_c) = 2.6$.[1] It follows that

$$B_c(L > L_c)/T = 30.6(N/10^{12}\ \mathrm{cm}^{-2}). \tag{4a}$$

For $L < L_c$, the Lande g factor is not yet known. A first measurement[22] of the magnetoresistance of a sample with $L = 40$ Å and $N \approx 1 \times 10^{12}$ cm^{-2} in a parallel magnetic field suggests that $g^*(L < L_c) \approx 6.5$. Therefore, we expect that

$$B_c(L < L_c)/T = 42.4(N/10^{12}\ \mathrm{cm}^{-2}). \tag{4b}$$

At low electron density, the critical fields are quite low and experiments should be easily feasible. We suggest to do transport measurements with AlP quantum wells in a parallel magnetic field in order to study many-body effects.

AlP samples, where one can change the electron density by a gate, would be very interesting, and comparison with our theoretical prediction would be simplified due to the fixed impurity density in such samples. Samples where one can change the electron density with light are also useful, but there one needs assumptions on how the impurity concentration chances with light.

Finally, we want to stress that the large effective electron mass m^* in AlP allows us to study strongly correlated electron systems with "high" electron densities in the range

10^{11} cm$^{-2} < N < 10^{12}$ cm^{-2}, see Fig. 1. This will help us better understand many-body effects in the two-dimensional disordered Coulomb system.

VII. CONCLUSION

For the two-dimensional electron gas realized in AlP, we presented theoretical results for the transport time, the Dingle temperature, and the resistivity in a parallel magnetic field. We conclude that AlP quantum wells represent a very interesting system to study interface-roughness scattering, many-body effects, and localization effects in thin quantum wells when $L < L_c$. This could be used to get information about the roughness parameters Δ and Λ of the AlP surface.

AlP quantum wells with $L < L_c$ and $L > L_c$ should be studied with a parallel magnetic field in order to get information about many-body effects in the density range 5×10^{10} cm$^{-2} < N < 5 \times 10^{12}$ cm^{-2}. Measurements of the transport scattering time and the single-particle relaxation time allow us to determine microscopic parameters of disorder and the real doping profile in the sample.

*Author to whom correspondence should be addressed.

[1] M. P. Semtsiv, S. Dressler, W. T. Masselink, V. V. Rylkov, J. Galibert, M. Goiran, and J. Léotin, Phys. Rev. B **74**, 041303(R) (2006).
[2] M. P. Semtsiv, U. Müller, W. T. Masselink, N. Georgiev, T. Dekorsy, and M. Helm, Appl. Phys. Lett. **89**, 184102 (2007).
[3] M. Shayegan, E. P. Poortere, O. Gunawan, Y. P. Shkolnikov, E. Tutuc, and K. Vakili, Phys. Status Solidi B **243**, 3629 (2006).
[4] T. Ando, A. B. Fowler, and F. Stern, Rev. Mod. Phys. **54**, 437 (1982).
[5] M. Goiran, M. P. Semtsiv, S. Dressler, W. T. Masselink, J. Galibert, G. Fedorov, D. Smirnov, V. V. Rylkov, and J. Leotin, Proceedings of the 13th International Conference Narrow Gap Semiconductors, NGS 13, Guildford, UK, 2007 [Springer Proc. Phys. (to be published)].
[6] A. Gold, Solid State Commun. **60**, 53 (1986).
[7] A. Gold, Phys. Rev. B **35**, 723 (1987).
[8] S. Das Sarma and F. Stern, Phys. Rev. B **32**, 8442 (1985).
[9] A. Gold, Phys. Rev. B **38**, 10798 (1988).
[10] M. Jonson, J. Phys. C **9**, 3059 (1976); A. Gold, Phys. Rev. B **50**, 4297 (1994); Z. Phys. B: Condens. Matter **103**, 491 (1997); for a review, see K. S. Singwi and M. P. Tosi, Solid State Phys. **36**, 177 (1981).
[11] V. T. Dolgopolov and A. Gold, JETP Lett. **71**, 27 (2000); A. Gold and V. T. Dolgopolov, Physica E (Amsterdam) **17**, 280 (2003).
[12] H. Sakaki, T. Noda, K. Hirakawa, M. Tanaka, and T. Matsusue, Appl. Phys. Lett. **51**, 1934 (1987).
[13] R. Gottinger, A. Gold, G. Abstreiter, G. Weimann, and W. Schlapp, Europhys. Lett. **6**, 183 (1988).
[14] F. Szmulowicz, S. Elhamri, H. J. Haugan, G. J. Brown, and W. C. Mitchel, J. Appl. Phys. **101**, 043706 (2007).
[15] A. Gold and R. Marty, in *Proceedings of the MSS 13*, in Genova, Italy, July 2007, Physica E (Amsterdam), (to be published).
[16] A. Gold and W. Götze, Phys. Rev. B **33**, 2495 (1986); A. Gold, Appl. Phys. Lett. **54**, 2100 (1989); Phys. Rev. B **44**, 8818 (1991).
[17] A. Gold, JETP Lett. **72**, 401 (2000).
[18] A. A. Shashkin, M. Rahimi, S. Anissimova, S. V. Kravchenko, V. T. Dolgopolov, and T. M. Klapwijk, Phys. Rev. Lett. **91**, 046403 (2003).
[19] H.-I. Cho, G. M. Gusev, Z. D. Kvon, V. T. Renard, J.-H. Lee, and J.-C. Portal, Phys. Rev. B **71**, 245323 (2005).
[20] S. V. Kravchenko and M. P. Sarachik, Rep. Prog. Phys. **67**, 1 (2004).
[21] A. A. Shashkin, Phys. Usp. **48**, 129 (2005).
[22] M. Goiran (private communication). The density of the sample must be verified by a second measurement, however.